

Article

# Effect of Wind Turbine Blade Rotation on Triggering Lightning: An Experimental Study

Xishan Wen, Lu Qu, Yu Wang, Xiaoyue Chen \*, Lei Lan, Tianjun Si and Jianwei Xu

School of Electrical Engineering, Wuhan University, Wuhan 430072, China; xswen@whu.edu.cn (X.W.); ql26333@163.com (L.Q.); yuwang@whu.edu.cn (Y.W.); leilan69@163.com (L.L.); stj2015025@163.com (T.S.); x361294@163.com (J.X.)

\* Correspondence: chenxiaoyue@whu.edu.cn; Tel.: +86-27-6877-2285

Academic Editor: Frede Blaabjerg

Received: 2 October 2016; Accepted: 28 November 2016; Published: 7 December 2016

**Abstract:** Compared with other lightning targets on the ground, the most notable feature of a wind turbine is that the blades are usually in a rotating state when lightning strikes. To study the mechanism of blade rotation influencing wind turbine on triggering lightning, lightning discharge comparison tests based on a typical 2-MW 1:30-scaled wind turbine model with an arching high-voltage electrode were conducted under different modes of stationary and rotating blades. Negative polarity switching impulses of 250/2500  $\mu$ s were applied to the arching electrode. The up-and-down method was adopted for 50% discharge voltage and the discharge process was observed. The experimental results showed that under the condition of a 4 m gap, the breakdown voltage decreases and the connection point of the leaders approaches the high-voltage electrode with increasing blade speed, indicating that the wind turbine's blade rotation enhances the triggering of lightning. The analysis showed that the blade rotation could be altering the charge distribution on the blade tip, resulting in varied ascending leader development on the blade tip, which affected the discharge development process.

**Keywords:** wind turbine; blade; rotation; scaled test; up-and-down method

## 1. Introduction

With the development of wind power generation technology, the capacity of wind turbine units is gradually increasing. The length of wind turbine blades has increased to over 80 m, and the height of the blade tip from the ground has been increased to over 220 m, which increases the probability of wind turbines being struck by lightning [1,2]. This increase in lightning activity is especially significant in places where winter lightning activity occurs as reported in Japan and Europe during the winter season [3,4]. Wind turbine blades are likely in a rotating state when lightning strikes, and the ion distribution around the blade tips is similar to that around static high towers in strong wind conditions. The corona current of a static high tower varies with wind speed [5,6]; therefore, the blade rotation may affect the process through which lightning is triggered. Rachidi et al. analyzed the similarities between rocket-triggered lightning and tall wind turbines under rotary conditions and suggested that the wind turbines might generate lightning on their own [7]. On the basis of our review of the literature on wind turbines, model-based testing of lightning discharge in laboratory settings and lightning strike observations at actual wind turbine farms have been the main research methods.

In laboratory settings, researchers have conducted many model tests of lightning discharge; although the lightning in model tests cannot completely simulate the characteristics of natural lightning, such tests have some similarities in discharging regulation and they can be reproduced; moreover, the results can provide some reference values [8–10]. Radičević and colleagues first investigated the influence of wind turbine blade rotation on the characteristics of atmospheric discharge [11–13]. The tests were conducted in a high-voltage laboratory, and the up-and-down method was applied to

determine the 50% breakdown standard switching voltage. The results indicated that, with a 2 m air gap, breakdown voltages were up to approximately 16% higher for a rotating scaled model than for a stationary scale model. Furthermore, it was recommended that under thunderstorm conditions, the rotational speed of wind turbine blades should not be decreased in an attempt to reduce the number of direct strikes on the wind turbine.

At actual wind farms, Montanyà et al. observed lightning by using a 3D lightning mapping array and high-speed video recorder. The results showed that under certain thunderstorm conditions, wind turbine blades can generate electric discharges at regular intervals of 3 s depending on the rotational speed. This periodic effect was not observed in static towers, indicating that the rotating effect may play a critical role [14]. Wilson et al. conducted an experiment in a wind farm and analyzed cloud-to-ground lightning data. The results indicated that wind turbines with a rotating blade tip height of 125 m have a larger attractive radius (276 m) than the expected (160–200 m) radius of stationary towers of similar height and an attractive radius equivalent to that of a nearby 231 m high radio tower [15]. Wang et al. used various lightning observation instruments to observe a wind turbine struck by lightning and a neighboring lightning protection tower; a comparison with a stationary windmill or tower of similar height revealed that the rotating windmill tended to have a higher chance of initiating an ascending leader. Thus, when a thunderstorm is overhead, the rotation of the windmill should be stopped [16].

In summary, the effect of rotation on the enhancement of lightning has been discussed and investigated. According to the scaled model test, the blade rotation weakens the lightning-triggering ability of wind turbines. However, this finding is inconsistent with observations at actual wind farms. Thus, there is no clear evidence that the number of lightning flashes increases significantly with the effect of rotation, and research on the influence of wind turbine blade rotation on lightning behavior needs to proceed further.

The present experimental study investigated the effect of rotation blades on triggering lightning in a wind turbine with a long air gap. Discharge tests in long air gaps (2 and 4 m) were conducted by applying a negative impulse of 250/2500  $\mu$ s. The effect of blade rotation on the characteristics of lightning discharge and the breakdown path were investigated. Finally, the physical interpretation of the blade rotation effect on the lightning discharge process was analyzed to elucidate the influence of blade rotation on triggering lightning.

## 2. Test Description

### 2.1. Test System Arrangement

Simulation tests of more than 400 lightning strikes were conducted outdoors in the ultra-high-voltage alternating current test base in China. Negative switching impulses of 250/2500  $\mu$ s were obtained from a 7.5 MV, 750 kJ, 25-stage impulse generator. The discharge voltages were measured using a capacitive divider. The practical test field is presented in Figure 1.

### 2.2. Experimental Set-Up

The experimental set-up is presented in Figure 2. The switching impulses were applied to a high-voltage electrode to simulate a descending lightning leader. A typical 1:30-scale 2-MW wind turbine model was adopted in this experiment. The gap distances between the high-voltage electrode and wind turbine blade tip were 2 and 4 m. According to the theory of similarity, the distances of 2 and 4 m correspond to striking distances of 60 and 120 m, respectively. The discharge path was recorded using a camera (Canon 5D MarkII, Tokyo, Japan), and the breakdown voltages were measured using an oscilloscope (Yokogawa DLM2054, Tokyo, Japan).

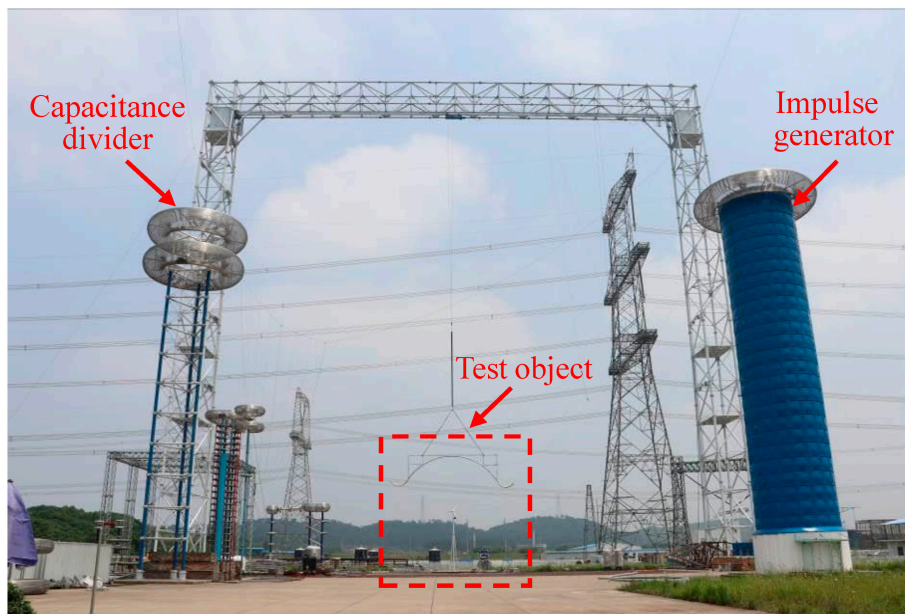


Figure 1. Arrangement of practical test field.

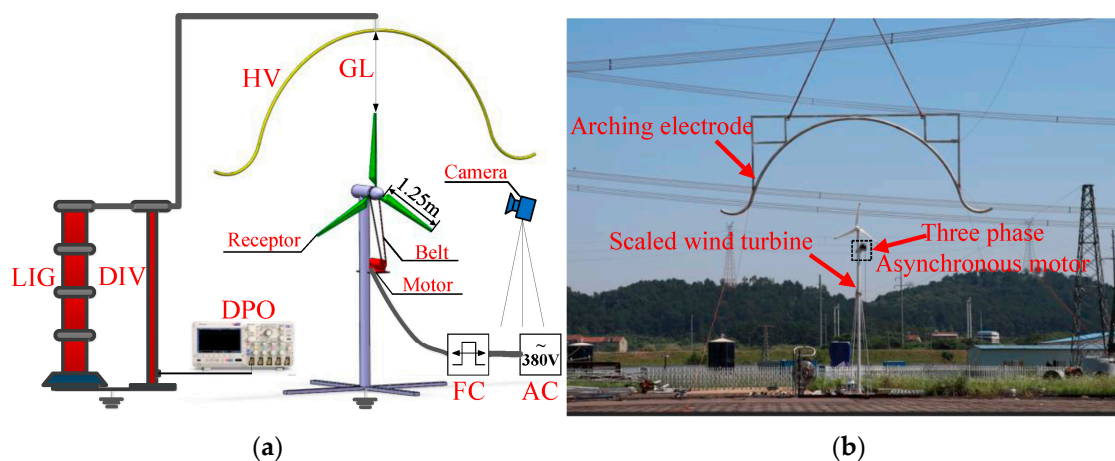


Figure 2. Test arrangement: (a) test model configuration; (b) diagram of scale model. AC: three-phase supply; DIV: capacitance divider; DPO: digital oscilloscope; FC: frequency converter; GL: gap length (2-m, 4-m); HV: high voltage arching electrode; LIG: lightning impulse generator.

### 2.3. High-Voltage Electrode

The high-voltage electrode selection is critical for investigating the influence of wind turbine blade rotation. To ensure that the distance between the rotation blade tip and high-voltage electrode was consistent, a special arching electrode was designed. The arching electrode mainly comprised a steel tube and a steel framework for preventing deformation of the steel tube. The steel tube was 159 mm in diameter and 5 mm in thickness. Considering an angle of  $120^\circ$  for each blade and the flashovers caused by the border effect, the arching electrode adopted an angle of  $150^\circ$ . Moreover, a reverse circular arc of  $110^\circ$  was arranged at the edge of the electrode. For the 2 m air gap, the radius of the arching electrode was 3.25 m, and the total length and weight exceeded 10 m and 260 kg, respectively. For the 4 m air gap, the radius of the arching electrode was 5.25 m, and the total length and weight exceeded 17 m and 700 kg, respectively. This design facilitated the generation of a quasi-uniform field above the blade by the arching electrode, which facilitated the development of streamers from the wind turbine model.

## 2.4. Scaled Wind Turbine Model

The three-blade scaled wind turbine model used in the experiment was a modified version of a small commercial wind turbine. To meet the experimental requirements, several aspects of the wind turbine were modified including wind turbine blade, power transmission module, and support component.

### 2.4.1. Wind Turbine Blade

The blades were made of a glass fiber-reinforced polymer composite insulating material and had a length of 1.25 m. Installing a lightning protection system (LPS) on the blades can effectively ground the lightning current and decrease the risk of lightning damage to the blade. Specifically, when the lightning discharge strikes the receptor on one of the blades, a surge current propagates through a down conductor over the blade, metallic cabin, bearings, and metallic tower to the grounding system.

The experiment adopted a typical LPS comprising the following:

- (1) Receptor (Figure 3a): receptors are isolated metal points on the blade tip (3 mm diameter circular copper 1 cm from the tip of the blade);
- (2) Down conductor: a 2.5 mm diameter copper down conductor embedded in the blade to connect the receptor to the metallic wind turbine hub.

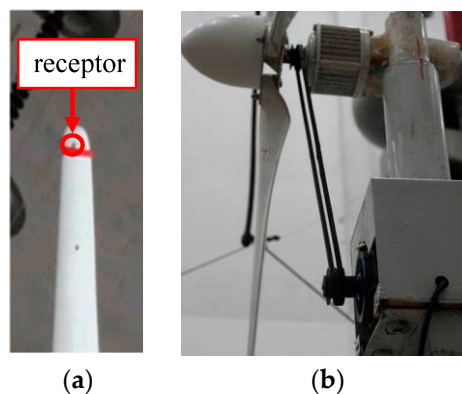


**Figure 3.** Diagram of typical receptors and power transmission module: (a) receptor; (b) Power transmission module.

### 2.4.2. Power Transmission Module

To ensure that the line speed of the scaled wind turbine blade tips was consistent with that of the actual operational wind turbine blade tips, a power transmission module was designed in this study, as shown in Figure 3b. The continuous speed regulation of the three-phase asynchronous motor was realized using a frequency converter; the asynchronous motor drives the wind turbine blades to rotate through the belt drive. A three-phase induction motor was placed in a Faraday cage near the top of the tower. The power of the motor was 2.2 kW, and the belt length was 1 m. To ensure the safety of the external power source, a surge protector was connected in parallel with the input of the frequency converter. Equation (1) presents the formula for simulating the line speed of the actual wind turbine blade tips:

$$w = \frac{30v}{\pi l}, \quad (1)$$

where  $v$  (m/s) is the line speed of the blade tips,  $w$  (r/min) is the rotational speed of the wind turbine blades, and  $l$  (m) is the length of the blade. When an actual wind turbine was operated with a rated power of 2 MW, the line speed of the turbine blade tips was approximately 60 m/s. Therefore, when the

wind turbine model simulated the rated operating condition of the actual wind turbine, the rotational speed  $w$  was 450 r/min.

### 2.4.3. Support Component

To ensure the stability of the rotating wind turbine, a support structure was designed in this study. The tower comprised a seamless steel tube with a height of 8 m and diameter of 245 mm. The cross angle steel composed the base of the wind turbine model.

### 2.5. Selection of Applied Waveform

A reasonable voltage waveform in a scaled wind turbine discharge test can reflect the characteristics of actual wind turbine discharge processes. Many researchers investigating the lightning discharge of ground objects have extensively applied a short-head-time (20–250  $\mu$ s) switching impulse to prevent a step leader from forming in the discharge process [8,10]. And according to IEC61400-24 [17], the 250/2500  $\mu$ s switching impulse waveform was recommended to achieve the lightning attachment manners of wind turbine blades. In the present study, the following parameters were considered for selecting the voltage waveform: the pause time between step leaders and the average electric field variation of objects on the ground.

The average electric field variation of objects on the ground can be obtained through electric field simulations. The applied waveform was selected to ensure that the average electric field variation caused by the impulse voltage was consistent with the electric field variation at the corona inception moment under natural conditions. Based on this method, the impulse voltage waveform was selected as 320/2500  $\mu$ s in a study by Xie et al. [18] and 200/2000  $\mu$ s in a study by Li et al. [19]. In the present study, the applied waveform was adopted from [19], and the variation under natural circumstances was calculated using Deller's leader progression model [20]. The settings of the simulation parameters are described as follows.

#### 2.5.1. Thundercloud

The simulation parameters of the thundercloud are as follows [19,21]:

- Suppose a unipolar negative charge (simplified condition) with a uniformly distributed extension of 10 km at a height of 2 km.
- Suppose an equivalent unipolar charge of 8 C.

#### 2.5.2. Descending Leader

For the method of describing the descending leader's channel, the charge density distribution equation proposed by Cooray and colleagues [20] was adopted, which is given by

$$\rho_s(\xi) = a_0 \left(1 - \frac{\xi}{H_c - z}\right) G(z) I_p + \frac{I_p (a + b\xi)}{1 + c\xi + d\xi^2} H(z), \quad (2)$$

in which

$$\begin{aligned} G(z) &= 1 - (z/H_c) \\ H(z) &= 0.3e^{-(z-10)/75} + 0.7G(z) \end{aligned} \quad '$$

where  $z$  is the height of the descending leader tip in meters,  $H_c$  is the height of the cloud in meters,  $I_p$  is the return stroke peak current in kilo-amperes, and  $\rho_s$  is the charge density in Coulomb per meter. The remaining coefficients were selected as follows:  $a_0 = 1.476 \times 10^{-5}$ ,  $\alpha = 4.857 \times 10^{-5}$ ,  $b = 3.9097 \times 10^{-6}$ ,  $c = 0.522$ , and  $d = 3.73 \times 10^{-3}$ . The speed of the descending leader was  $2 \times 10^5$  m/s.

### 2.5.3. Calculation of Electric Field on the Receptor Surface

According to the aforementioned considerations and assumptions, the field variation ( $S_c$  in kV/m/s) of the receptor on the blade tip at the corona inception moment was calculated using Equation (3) [19]:

$$s_c = \frac{(E_{t_{peak}+\Delta t} - E_{t_{peak}})}{\Delta t}, \quad (3)$$

where  $t_{peak}$  is the corona inception moment in the receptor on the blade tip and  $\Delta t = 8 \mu\text{s}$ .

The finite element software COMSOL Multiphysics 5.0 (COMSOL, Stockholm, Sweden) was used to calculate the electric field, and the simulation steps of the descending leader were set using MATLABR2014a (MathWorks, Natick, MA, USA). The simulation parameters in the model were as follows:

- Tower height: 90 m,
- Blade length: 40 m,
- Ground size: 500 m  $\times$  500 m  $\times$  1 m,
- Receptor diameter: 5 cm,
- Thundercloud height: 2 km.

For the scaled wind turbine model, a simplified model based on these parameters was arranged using the finite element software. The average field variation ( $S_e$  in kV/m/s) at the receptor in the scaled model test was calculated using Equation (4) [19]:

$$s_e = \frac{(E_{90\%} - E_{10\%})}{(t_{90\%} - t_{10\%})}, \quad (4)$$

where  $E_{90\%}$  and  $E_{10\%}$  are the electric field strengths of the receptor in the scaled model when the arching electrode potential is 90% and 10% of the impulse waveform peak, respectively;  $t_{90\%}$  and  $t_{10\%}$  are the times at which the arching electrode potential is equal to 90% and 10% of the impulse waveform peak, respectively; and  $S_c$  and  $S_e$  are obtained from Equations (3) and (4). The field variations at various wavefront times are presented in Table 1.

**Table 1.** Comparison of variation under different wavefront times.

	$S_e$ (kV/m/ $\mu\text{s}$ )
Natural Lightning	22.11
1.2/50 $\mu\text{s}$	4942
80/2500 $\mu\text{s}$	74.13
250/2500 $\mu\text{s}$	23.72
1000/2500 $\mu\text{s}$	5.93

$S_e$ : average variation rate of surface electric field.

A comparison of the average electric field variation under natural lightning ( $S_c$ ) conditions with that under various waveform front times ( $S_e$ ) revealed that the negative 250/2500  $\mu\text{s}$  switching impulse was the most similar to natural lightning among the four waveforms. This waveform was recommended by IEC61400-24 [17] for lightning protection tests of the wind turbine. Therefore, a negative voltage waveform of 250/2500  $\mu\text{s}$  was selected for the test in the present study.

### 2.6. Test Procedure

The 50% breakdown voltage ( $U_{50\%}$ ) was obtained through the up-and-down method with a 3%–4% difference in the expected discharge voltage between steps, and 40 strokes were applied for each arrangement. The scaled model test was conducted under the following three wind turbine operating conditions:

- $w = 0$  r/min, with the wind turbine in the stationary status and the blades located in three typical positions ( $\theta = 0^\circ, 30^\circ, 60^\circ$ ), as shown in Figure 4.
- $w = 250$  r/min, with the wind turbine in the subsynchronous generation status, where the simulated natural wind speed is too low to generate power and the blades rotate at a medium speed.
- $w = 450$  r/min, with the wind turbine in the synchronous generation status and the model blades rotating at the rated speed.

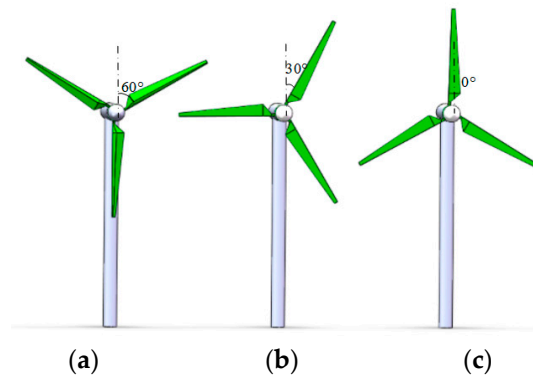


Figure 4. Typical position of static blade: (a)  $\theta = 60^\circ$ ; (b)  $\theta = 30^\circ$ ; (c)  $\theta = 0^\circ$ .

### 3. Test Results

#### 3.1. Test Data of Various Arrangements

All the tests in the present study were performed outdoors for a duration of one week in May 2016. Under all test conditions, the discharge struck the receptor directly. The test data were normalized using Equation (5):

$$U_{50\%}(\text{standard}) = \frac{U_{50\%}(\text{measured})}{\delta} \quad (5)$$

where  $\delta$  is the atmospheric correction factor to eliminate the effects of temperature, humidity, and pressure during the discharge processes [22].

During the tests, the temperature ranged from 21.4 to 31.6 °C, the relative humidity ranged from 52% to 80%, and the atmospheric pressure ranged from 99.8 to 100.9 kPa. The test results are presented in Table 2. Here,  $\sigma_{U_{50\%}}$  and  $\sigma_{T_f}$  represents discharge dispersivity, which equals the value of the standard deviation divided by the  $U_{50\%}$  and  $T_f$  of each arrangement, respectively.

Table 2. Breakdown characteristic of wind turbine.

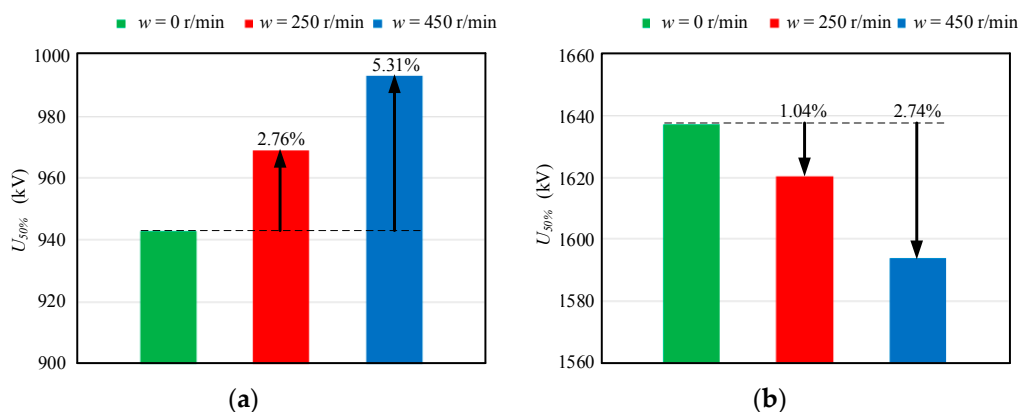
Gap Length	Blade Status	$\delta$	$U_{50\%}$ (kV)	$\sigma_{U_{50\%}}$ (%)	$T_f$ ( $\mu$ s)	$\sigma_{T_f}$ (%)	
2 m	static	$\theta = 0^\circ$	1.049	907.55	3.34	179.71	11.24
		$\theta = 30^\circ$	1.087	942.91	4.14	183.50	12.88
		$\theta = 60^\circ$	1.070	977.78	4.92	163.73	16.35
		$w = 0$ (average)	1.022	942.75	4.14	175.65	13.49
	rotatory	$w = 250$ r/min	1.035	968.76	3.95	178.69	26.92
		$w = 450$ r/min	1.049	992.78	5.59	167.86	29.61
4 m	static	$\theta = 0^\circ$	1.020	1594.42	5.27	149.00	10.74
		$\theta = 30^\circ$	1.012	1607.42	5.07	156.20	9.63
		$\theta = 60^\circ$	1.013	1710.06	3.75	166.93	29.21
		$w = 0$ (average)	1.015	1637.30	4.70	157.38	16.53
	rotatory	$w = 250$ r/min	1.009	1620.33	5.00	157.88	9.51
		$w = 450$ r/min	1.006	1593.53	4.73	163.60	26.49

### 3.2. Influence of Wind Turbine Blade Rotation on the Characteristics of Atmospheric Discharges

Derived from the  $U_{50\%}$  and  $T_f$  values in Table 2, the  $U_{50\%}$  and  $T_f$  ratios under various rotating speeds are shown in Table 3. From Table 3, the  $U_{50\%}$  ratio was plotted to obtain the relationship between  $U_{50\%}$  and the rotational speed in different air gaps and is shown in Figure 5.

**Table 3.** Relationship between  $U_{50\%}$  and  $T_f$  ratio under different rotating speeds.

Gap Length	$\frac{U_{50\%250rpm}}{U_{50\%0rpm}}$	$\frac{U_{50\%250rpm}}{U_{50\%0rpm}}$	$\frac{T_f250rpm}{T_f0rpm}$	$\frac{T_f450rpm}{T_f0rpm}$
	(p.u)	(p.u)	(p.u)	(p.u)
2 m	1.0276	1.0531	1.0173	0.9556
4 m	0.9859	0.9725	1.0032	1.0395



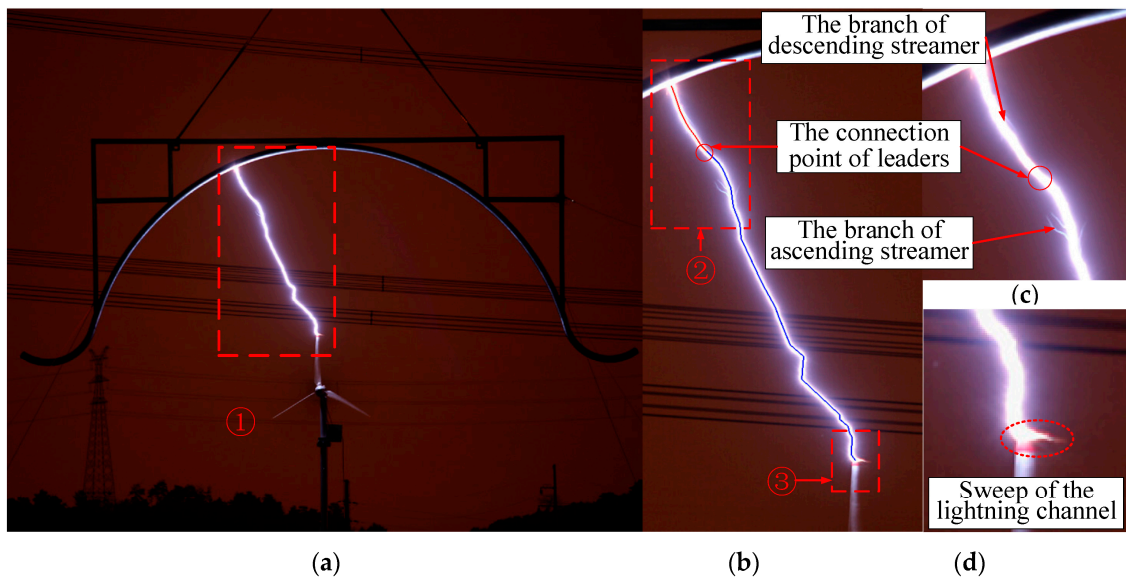
**Figure 5.** Relationship between  $U_{50\%}$  and  $w$  in different air gaps. (a) 2 m air gap; (b) 4 m air gap.

Table 3 and Figure 5 show that with an increase in blade rotation speed, the  $U_{50\%}$  between the blade tip and arching electrode presents different trends for these two air gaps. In addition, no marked regularity was observed in  $T_f$ . Furthermore, the effect of blade rotation on the gap breakdown characteristic is detailed in the following.

For the 2 m air gap, compared with the static condition of the wind turbine,  $U_{50\%}$  increased slightly by 2.76% (medium blade speed) and 5.31% (rated blade speed). For the 4 m air gap, as the blade rotation speed increased, the  $U_{50\%}$  variation regularity differed from that in the 2 m air gap arrangement. Compared with the static wind turbine condition, the average  $U_{50\%}$  value decreased slightly by 1.04% (medium blade speed) and 2.74% (rated blade speed). In addition, as the blade rotation speed increased,  $T_f$  increased slightly by 0.32% (medium blade speed) and 3.95% (rated blade speed).

### 3.3. Breakdown Path Characteristics

In all arrangement cases, the discharge development path was recorded through long-time camera exposure. The typical discharge process of the rotating wind turbine with the 4 m gap is presented in Figure 6. Moreover, natural lightning striking rotating wind turbine blades in Japan is illustrated in Figure 7b [23]. The morphological characteristics of the breakdown path presented in Figure 6d are similar to those in Figure 7, indicating that the laboratory test could reflect the process of natural lightning striking the rotating wind turbine to a certain extent.



**Figure 6.** The typical discharge process of the rotating wind turbine with the 4 m air gap. (a) overview of the breakdown path; (b) ascending leader and descending leader length measurement (enlargement/magnification of ①); (c) ascending leader and descending leader connection (enlargement/magnification of ②); (d) lightning discharge on the blade tip in the rotating process (enlargement/ magnification of ③).

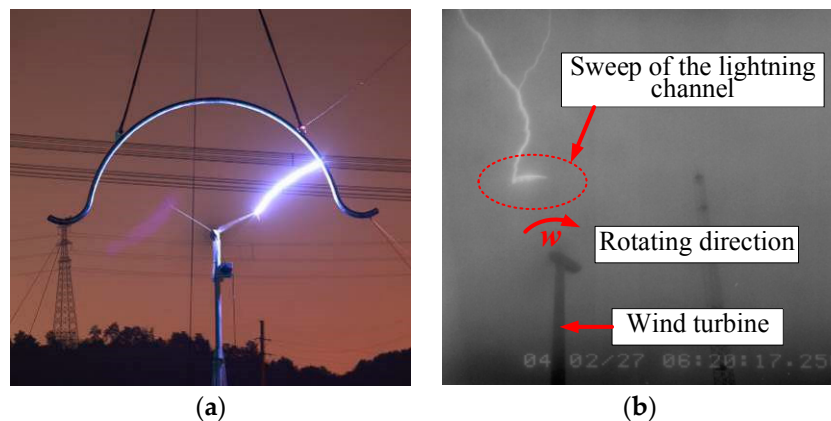


**Figure 7.** The typical discharge process of rotating wind turbine. (a) the breakdown path of scaled model test in 2 m air gap; (b) natural lightning striking rotating wind turbine blades in Japan.

Through the analysis of a typical breakdown path, the method for determining the leader connection point is proposed as follows. According to the theory of discharge in long air gaps, streamer discharges develop from the head of the leader channel. Therefore, the development of ascending and descending streamer branches was observed proximal to the connection point of the leaders. In the interval between the two streamers, the apparent bending parts of the breakdown path represented the leader connection point.

After the leader connection point was determined, the length of the ascending and descending leaders in each arrangement of lightning discharge tests was measured using Autodesk Design Review 2013 (Autodesk, San Rafael, CA, USA). As shown in Figure 6b, the ascending and descending leaders developed from the arching electrode and blade receptor, respectively, and terminated at the leader connection point. The breakdown path is depicted using a multiline segment. The red line segment represents the descending leader and the blue line segment represents the ascending leader. The

ascending and descending leader lengths at various blade rotation speeds under the gap breakdown conditions are presented in Table 4.

**Table 4.** The length of ascending and descending leaders under different blade statuses.

Gap Length	Blade Status	Descending Leader Length (m)	Ascending Leader Length (m)	Descending/Ascending Leader Length Ratio (%)	
2 m	static	$\theta = 0^\circ$	0.54	1.63	32.7
		$\theta = 30^\circ$	0.51	1.62	31.1
		$\theta = 60^\circ$	0.41	1.73	24
		$w = 0$ (average)	0.49	1.66	29.17
	rotatory	$w = 250$ r/min	0.51	1.64	30.94
		$w = 450$ r/min	0.55	1.60	34.16
4 m	static	$\theta = 0^\circ$	1.01	3.33	30.33
		$\theta = 30^\circ$	1.04	3.26	31.90
		$\theta = 60^\circ$	1.08	3.17	34.07
		$w = 0$ (average)	1.04	3.25	32.00
	rotatory	$w = 250$ r/min	0.97	3.30	29.39
		$w = 450$ r/min	0.94	3.34	28.14

From the results in Table 4, the relationship between the leader length and rotational speed with various receptors was plotted (Figure 8), and the effect of blade rotation on the leader length was analyzed in detail.

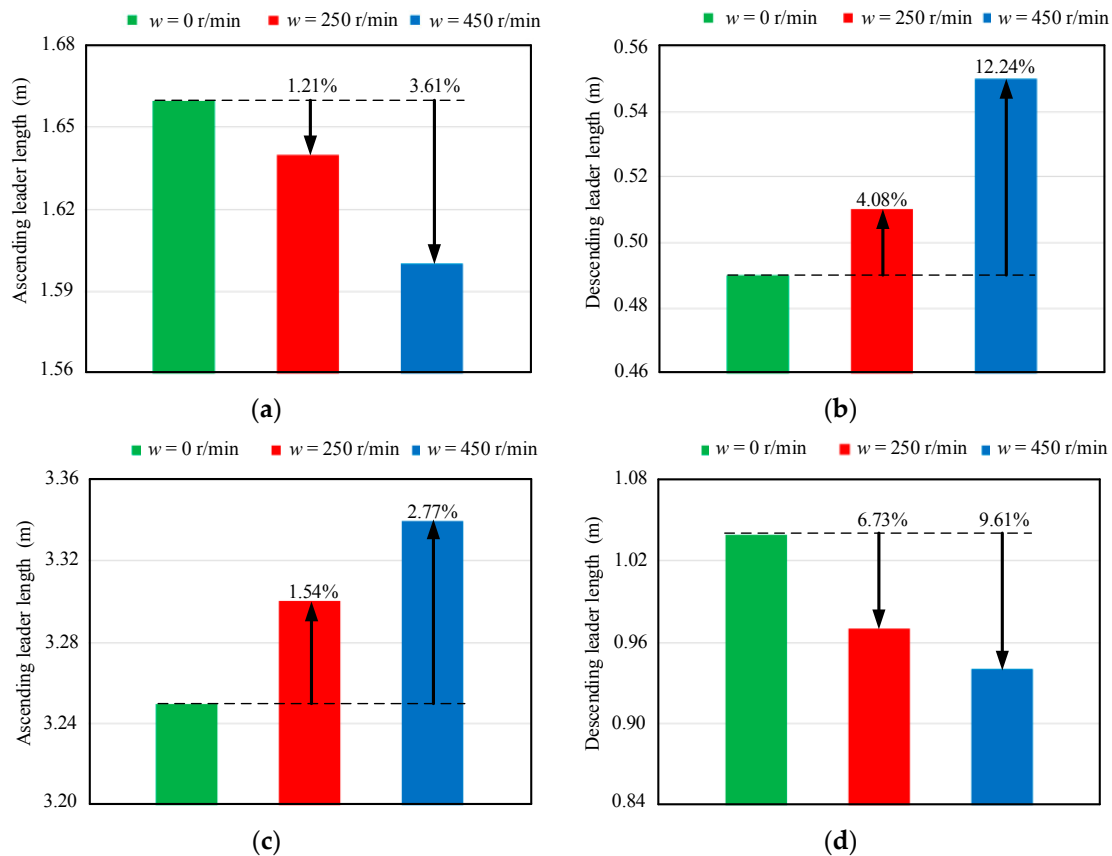


**Figure 8.** Relationship between the leader length and rotation speed in different air gap. (a) ascending leader length in 2 m air gap; (b) descending leader length in 2 m air gap; (c) ascending leader length in 4 m air gap; (d) descending leader length in 4 m air gap.

For the 2 m air gap, compared with the static wind turbine condition, the length of the ascending leader decreased slightly by 1.21% (medium blade speed) and 3.61% (rated blade speed), and that of the descending leader increased slightly by 4.08% (medium blade speed) and 12.24% (rated blade speed). For the 4 m air gap, as the blade rotation speed increased, the leader length variation regularity differed from that in the 2 m air gap arrangement. Compared with the static wind turbine condition, the length of the ascending leader increased slightly by 1.54% (medium blade speed) and 2.77% (rated blade speed), and that of the descending leader decreased slightly by 6.73% (medium blade speed) and 9.61% (rated blade speed).

#### 4. Physical Interpretation of the Blade Rotation Effect in the Lightning Discharge Process

##### 4.1. Summary of the Test Results

To verify the objectiveness of the test results, they were compared with those of a study by Radičević [13]. In Radičević's study, the test was conducted under three wind turbine operating conditions ( $v = 0$  m/s with one blade straight up,  $v = 31$  m/s, and  $v = 50$  m/s;  $v$  is the linear velocity of the blade tip, which was calculated using Equation (1)) with the same impulse voltage waveform and test method used in the present study. As the rotation speed increased, the  $U_{50\%}$  of the scaled model increased by 2.85% (medium blade speed) and 9.41% (rated blade speed) relative to that of the stationary model, as shown in Figure 9a. In the present study, for the 2 m gap, three wind turbine operating conditions were selected ( $v = 0$  m/s with one blade straight up,  $v = 33$  m/s, and  $v = 60$  m/s). As the rotation speed increased, the  $U_{50\%}$  of the rotating scaled model increased by 6.17% (medium blade speed) and 9.39% (rated blade speed) relative to that of the stationary model. The results in Table 2 are plotted in Figure 9b. In conclusion, the results of the present study exhibited a similar trend to those in the study of Radičević; specifically, when the blades were rotating, an increase in  $U_{50\%}$  was recorded, and the connection points of the leaders from the arching electrode and corresponding blade approached the blade tip.

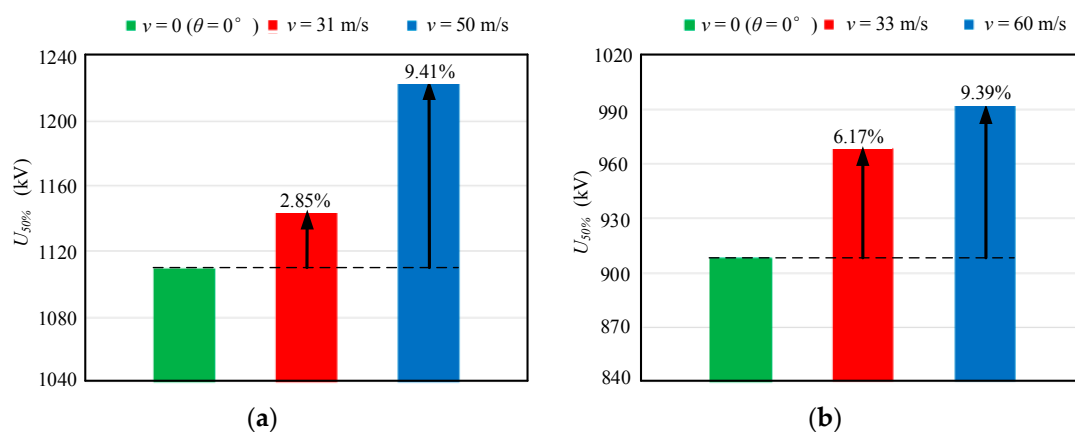


**Figure 9.** Relationship between  $U_{50\%}$  and  $v$  in 2 m air gap. (a) test results in [13]; (b) test results in the present paper;  $v = 0$  ( $\theta = 0^\circ$ ): one blade is straight up.

The results differed markedly from those of the 4 m air gap test; in that test, as the blade rotation speed increased, the  $U_{50\%}$  between the corresponding blade tip and high-voltage electrode exhibited an increasing trend and the leader connection point approached the arching electrode, which means that the ascending leader developed more adequately.

A comparison of the test results at the different gap lengths revealed that the trend in  $U_{50\%}$  and the connection points of leaders varied as the blade rotation speed increased, indicating that the physical lightning discharge processes at different gap lengths vary under different blade rotation conditions. The specific situation is analyzed in the following section.

#### 4.2. Effect of Blade Rotation on the Lightning Discharge Process

In the standard atmospheric environment, if the initial field strength is 10 kV/cm, the average speed of electrons in the air gap is approximately 0.1 m/ $\mu$ s, whereas that of the positive ions is approximately  $10^{-4}$  m/ $\mu$ s. In the present study, the maximum speed of the blade tip was approximately  $0.6 \times 10^{-4}$  m/ $\mu$ s [24]. Therefore, the electron speed was higher than the blade tip speed by four orders of magnitude, and the influence of the distribution of electrons under blade rotation can be ignored. However, the maximum speed of the blade tip and the positive ion speed were of the same order of magnitude, indicating that blade rotation influenced the distribution of positive ions. The lightning discharge process of the wind turbine blades under stationary and rotating conditions is analyzed in detail as follows.

As shown in Figure 10, a negative 250/2500  $\mu$ s waveform was applied to the high-voltage electrode, and the blade tip presented relatively positive. When the blade rotation speed was  $w = 0$ , air ionization occurred because of the high electric field strength. Because of the high drift velocity of the ionized electrons, the electrons rapidly entered the receptor of the blade tip. Positive ions remained near the blade tip and were distributed along the highest electric field with a drift velocity ( $\mu E$ ). When the blade rotation speed was  $w > 0$ , the distribution of the ionized positive ions near the blade tip was influenced simultaneously by the electric field and blade rotation. Because of the blade rotation, the corona charge  $q_c$  was distributed in layers with a density of  $\rho_c$  above the blade tip. The discharge process was altered by the corona in two aspects. First, the electric field strength ( $E_{\rho c 2}$ ) of the tip area was weakened by the positive ion region, thereby inhibiting the formation of new coronas and leaders. By contrast, the outside electric field strength ( $E_{\rho c 1}$ ) was enhanced outside the positive ion region, which was conducive to the development of the ascending leader.

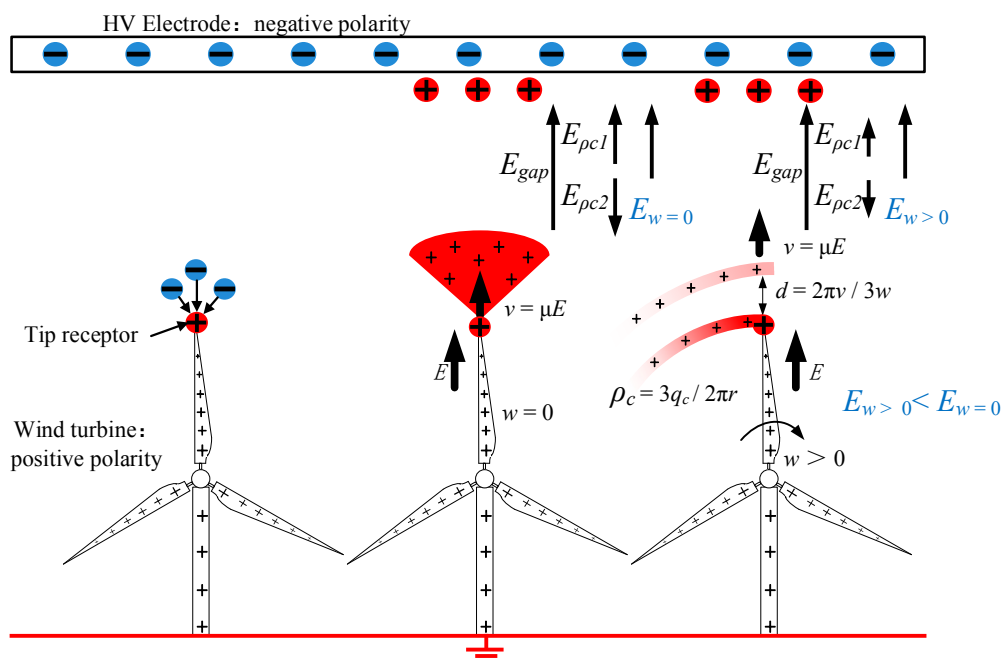


**Figure 10.** Schematic diagram of space charge distribution in static and rotating wind turbine. (refer to reference [14]).  $E_g$ : electric field strength of the gap;  $E_{\rho c 1}$ : electric field strength outside of the tip area;  $E_{\rho c 2}$ : electric field strength of the tip area;  $E_{w=0}$ : overall intensity of the applied electric field under  $w = 0$  r/min;  $E_{w>0}$ : overall intensity of the applied electric field under  $w > 0$  r/min;  $\rho_c$ : charge density near the blade tip;  $v$ : the drift velocity of the positive ions.

When the gap distance was short (2 m in present test), the main effect was that the positive space charge altered the discharge process by increasing the outside electric field strength ( $E_{\rho c 1}$ ). When the

blade rotation speed was  $w > 0$ , the positive space charge density decreased, and the enhancement effect of the outside electric field strength ( $E_{\rho c1}$ ) was mitigated. Therefore, with the increase in blade rotation speed, it was more difficult for ascending leaders to develop, the leader length became shorter, and the breakdown voltage was higher. When the gap distance was long (4 m in present test), the enhancement effect of the positive space charge accumulation on the outside electric field strength ( $E_{\rho c1}$ ) was clearly decreased. Under this condition, the main effect was that the positive space charge altered the discharge process by reducing the electric field strength ( $E_{\rho c2}$ ) of the tip area, thereby inhibiting the formation of new coronas and leaders. When the blade rotation speed was  $w > 0$ , the positive space charge density decreased, ascending leaders developed more easily, the ascending leader length was longer, and the breakdown voltage was lower.

The test results and theoretical analysis demonstrated that when the wind turbine blades were rotating, the positive space charge distribution at the tip area differed from those observed under the stationary condition. The blade rotation altered the breakdown voltage and ascending leader length and influenced the attached lightning capacity of the wind turbine. The effect of the blade rotation on the attached lightning capacity varied with the gap distance.

## 5. Conclusions

This paper presents the lightning discharge behavior in rotating wind turbines, which was determined through scaled model tests with 2 m and 4 m air gaps. The test results reflected some discharge behaviors that occur in actual lightning discharge processes. On the basis of the findings, the following conclusions can be drawn:

1. In the 2 m air gap test, with an increase in the blade rotation speed, the breakdown voltage between the blade tip and arching electrode presented a slightly increasing trend, and the connection points of leaders from the arching electrode and rotating blade moved slightly closer to the blade tip.
2. In the 4 m air gap test, with an increase in the blade rotation speed, the breakdown voltage between the blade tip and arching electrode presented a slightly decreasing trend. Moreover, the ascending leader developed more adequately, and the connection points of leaders from the arching electrode and rotating blade moved slightly closer to the arching electrode.
3. In the 4 m air gap test, the blade rotation altered the charge distribution on the blade tip region and favored the initiation of lightning, which is in agreement with observations at actual wind farms. However, for the 2 m air gap test, a small-scale test was insufficient for extrapolating the test results to practical cases because of the nonlinear discharge characteristics of long air gaps. To obtain more practical results, large-scale tests are warranted.
4. It is reasonable to consider that there is a difference in the triggering of lightning depending on whether the blades are rotating. Numerical software methods must be applied to account for blade rotation for predicting possible attachment points on wind turbines.

**Acknowledgments:** The authors would like to thank the reviewers of this paper for the useful comments. This work is supported by the China State Grid Corp headquarters project in 2015 (SGTYHT/14-JS-188). The authors also would like to particularly thank Qiming Ye and Yeming Ma (China Electric Power Research Institute, China) for their consistent support throughout the experiment procedure.

**Author Contributions:** Xishan Wen, Lu Qu, Yu Wang and Lei Lan conceived and designed the experiments; Lu Qu, Tianjun Si and Jianwei Xu performed the experiments; Lu Qu, Yu Wang, Tianjun Si and Xiaoyue Chen analysed the data; Lu Qu and Tianjun Si contributed reagents/materials/analysis tools; Lu Qu, Yu Wang, Xiaoyue Chen and Tianjun Si wrote the paper.

**Conflicts of Interest:** The authors declare no conflict of interest.

## References

1. Montanyà, J.; Fabró, F.; van der Velde, O.; March, V.; Williams, E.R.; Pineda, N.; Romero, D.; Solà, G.; Freijo, M. Global distribution of winter lightning: A threat to wind turbines and aircraft. *Nat. Hazards Earth Syst. Sci.* **2016**, *16*, 1465–1472. [[CrossRef](#)]
2. Garolera, A.C.; Madsen, S.F.; Nissim, M.; Myers, J.; Holboell, J. Lightning Damage to Wind Turbine Blades From Wind Farms in U.S. *IEEE Trans. Power Deliv.* **2014**, *31*, 1043–1049. [[CrossRef](#)]
3. Wada, A.; Yokoyama, S.; Hachiya, K.; Hirose, T. Observational results of lightning flashes on the Nikaho-Kogen wind farm in winter (2003–2004). In Proceedings of the XIV International Symposium on High Voltage Engineering, Beijing, China, 25–29 August 2005; p. 86.
4. March, V. Upward lightning observations on a wind turbine and its implications to environmental factor for risk assessment. In Proceedings of the Asia-Pacific Conference Lightning Protection, Nagoya, Japan, 23–27 June 2015; pp. 31–35.
5. Diaz, J.; Ocampo, G.; Chaves, S.; Román, F. Positive and Negative Point Discharge Corona Currents: Influence of Thunderstorm-like Wind Velocities. In Proceedings of the 2014 IEEE International Conference on Lightning Protection (ICLP), Shanghai, China, 11–18 October 2014; pp. 1552–1555.
6. Bazelyan, E.M.; Raizer, Y.P.; Aleksandrov, N.L.; D'Alessandro, F. Corona processes and lightning attachment: The effect of wind during thunderstorms. *Atmos. Res.* **2009**, *94*, 436–447. [[CrossRef](#)]
7. Rachidi, F.; Rubinstein, M.; Montanya, J.; Bermudez, J.L.; Sola, R.R.; Sola, G.; Korovkin, N. A Review of Current Issues in Lightning Protection of New-Generation Wind Turbine Blades. *IEEE Trans. Ind. Electron.* **2008**, *55*, 2489–2496. [[CrossRef](#)]
8. Wang, Y.; Wen, X.; Lan, L.; An, Y.; Dai, M.; Gu, D.; Li, Z. Breakdown characteristics of long air gap with negative polarity switching impulse. *IEEE Trans. Dielectr. Electr. Insul.* **2014**, *21*, 603–611. [[CrossRef](#)]
9. Taniguchi, S.; Okabe, S. A Contribution to the Investigation of the Shielding Effect of Transmission Line Conductors to Lightning Strikes. *IEEE Trans. Dielectr. Electr. Insul.* **2008**, *15*, 710–720. [[CrossRef](#)]
10. Taniguchi, S.; Okabe, S.; Takahashi, T.; Shindo, T. Air-Gap Discharge Characteristics in Foggy Conditions Relevant to Lightning Shielding of Transmission Lines. *IEEE Trans. Power Deliv.* **2008**, *23*, 2409–2416. [[CrossRef](#)]
11. Radičević, B.M.; Savić, M.S.; Badea, I. Impact of wind turbine blade rotation on the lightning strike incidence. In Proceedings of the 2012 IEEE International Conference on Lightning Protection (ICLP), Vienna, Austria, 2–7 September 2012; pp. 1–9.
12. Radičević, B.M.; Savić, M.S.; Madsen, S.F.; Badea, I. Impact of wind turbine blade rotation on the lightning strike incidence—A theoretical and experimental study using a reduced-size model. *Energy* **2012**, *45*, 644–654. [[CrossRef](#)]
13. Radičević, B.M.; Savić, M.S. Experimental Research on the Influence of Wind Turbine Blade Rotation on the Characteristics of Atmospheric Discharges. *IEEE Trans. Energy Convers.* **2011**, *26*, 1181–1190. [[CrossRef](#)]
14. Montanyà, J.; van der Velde, O.; Williams, E.R. Lightning discharges produced by wind turbines. *J. Geophys. Res. Atmos.* **2014**, *119*, 1455–1462. [[CrossRef](#)]
15. Wilson, N.; Myers, J.; Cummins, K.; Hutchinson, M.; Nag, A. Lightning attachment to wind turbines in central Kansas: Video observations, correlation with the NLDN and in-situ peak current measurements. In Proceedings of the European Wind Energy Association Annual Event, Vienna, Austria, 4–7 February 2013; pp. 1–8.
16. Wang, D.; Takagi, N.; Watanabe, T.; Sakurano, H.; Hashimoto, M. Observed characteristics of upward leaders that are initiated from a windmill and its lightning protection tower. *Geophys. Res. Lett.* **2008**, *35*, 1–5. [[CrossRef](#)]
17. International Electrotechnical Commission. *Wind Turbines Part 24: Lightning Protection*, 1st ed.; IEC 61400-24, International Standard; IEC: Geneva, Switzerland, 2010.
18. Xie, S.J. Simulation Tests and Models of the Selection Process in Negative Cloud-to-Ground Lightning Flash. Ph.D. Thesis, Huazhong University of Science & Technology, Wuhan, China, 2013.
19. Li, Z.; Zeng, R.; Yu, Z.; Chen, S.; Liao, Y.; Li, R. Research on the upward leader emerging from transmission line by laboratory experiments. *Electr. Power Syst. Res.* **2013**, *94*, 64–70. [[CrossRef](#)]
20. Becerra, M.; Cooray, V. A Simplified Physical Model to Determine the Lightning Upward Connecting Leader Inception. *IEEE Trans. Power Deliv.* **2006**, *21*, 897–908. [[CrossRef](#)]

21. Uman, M.A. *The Lightning Discharge*; Academic Press: San Diego, CA, USA, 1987; pp. 58–66.
22. International Electrotechnical Commission. *High-Voltage Test Techniques—Part 1: General Definitions and Test Requirements*, 3rd ed.; IEC 60060-1; IEC: Geneva, Switzerland, 2010.
23. Yokoyama, S. Lightning protection of wind turbine blades. *Electr. Power Syst. Res.* **2013**, *94*, 3–9. [[CrossRef](#)]
24. Aleksandrov, N.L.; Bazelyan, E.M.; Drabkin, M.M.; Carpenter, R.B., Jr.; Raizer, Y.P. Corona Discharge at the Tip of a Tall Object in the Electric Field of a Thundercloud. *Plasma Phys. Rep.* **2002**, *28*, 1032–1045. [[CrossRef](#)]



© 2016 by the authors; licensee MDPI, Basel, Switzerland. This article is an open access article distributed under the terms and conditions of the Creative Commons Attribution (CC-BY) license (<http://creativecommons.org/licenses/by/4.0/>).